Resonant-tunneling spectroscopy of coupled hole subbands in strained Si/SiGe triple-barrier structures

B. Ferland
Division of Engineering, Brown University, Providence, Rhode Island 02912

C. D. Akyüz
Department of Physics, Brown University, Providence, Rhode Island 02912

A. Zaslavsky
Division of Engineering, Brown University, Providence, Rhode Island 02912

T. O. Sedgwick
SiBond L. L. C., Hudson Valley Research Park, Hopewell Junction, New York 12533
(Received 22 August 1995)

We examine transport of holes in asymmetric triple-barrier p-Si/$Si_{0.8}Ge_{0.2}$ resonant tunneling structures with different middle barrier widths ($L=10$, 20, and 30 Å) for $T\leqslant 4.2$ K. The two-dimensional (2D) heavy-hole (HH) and light-hole (LH) subbands in each of the two quantum wells interact through interwell tunneling, resulting in 2D double-well subbands. We identify resonances corresponding to tunneling transitions through these double-well subbands using a simple wave-function formalism. The observed resonances correspond to strong HH-HH coupling with the addition of weaker HH-LH coupling for the narrowest middle barrier width, $L=10$ Å. We also present measurements displaying the HH-LH interaction strength dependence on high magnetic fields parallel to the current, $B_{\|}$. The weak HH-LH interaction quenches as $B_{\|}$ approaches 10 T.

Recent advances in strained silicon epitaxy have allowed for the creation of high quality $Si/Si_{1-x}Ge_x$ heterostructures.[1,2] One of the principal directions in $Si/Si_{1-x}Ge_x$ heterostructure research is the study of p-type double-barrier resonant tunneling structures (RTS's).[3–6] The interaction of heavy-hole (HH) and light-hole (LH) valence subbands in p-type quantum wells complicates the study of hole tunneling compared to the well-understood electron resonant tunneling in III-V double-barrier RTS's.[7–9] In p-$Si/Si_{1-x}Ge_x$ quantum-well structures, strain and quantum confinement create two-dimensional (2D) HH and LH subbands with different in-plane dispersion relations, $E_i(\mathbf{k}_\perp)$. These in-plane dispersions are further complicated by subband interactions whenever the energy separation of various subbands is small,[10,11] resulting in nonparabolic and anisotropic $E_i(\mathbf{k}_\perp)$. Measurements of p-Si/SiGe double-barrier RTS's have probed the heavy- and light-hole in-plane dispersion relations extensively.[12,13] A simple two-band nonparabolic model[13] adequately describes the lowest-lying HH_0 subband. The analysis of the LH_0 subband is more complicated due to strong interactions with the lower-lying HH_0 subband along with nearby higher-energy subbands and continuum states.

Triple-barrier RTS's, in which two quantum wells are separated by a narrow middle tunneling barrier,[14] are of interest in p-type RTS's because current transport proceeds via tunneling through coupled 2D HH-HH and HH-LH subbands. In this paper we present measurements of transport and magnetotransport in p-$Si/Si_{0.8}Ge_{0.2}$ triple-barrier RTS's with various middle barrier widths L, where we observe resonant peaks due to tunneling through coupled hole subbands. Using a simple wave-function formalism, we identify the origin of these peaks, including a peak due to HH-LH coupling in the structure with the narrowest middle barrier width $L=10$ Å. We also present magnetotunneling data which exhibit quenching of the observed HH-LH interaction in high magnetic fields parallel to the current, $B_{\|}\geqslant 10$ T.

The triple-barrier RTS's used for these measurements were grown by atmospheric pressure chemical vapor deposition on silicon substrates.[15] The active region consists of two undoped $Si/Si_{0.8}Ge_{0.2}$ wells with nominal widths $W_1=35$ Å and $W_2=28$ Å separated by a narrow middle barrier of undoped Si of nominal width $L=10$, 20, and 30 Å for the three different structures and clad by 35-Å outer barriers of undoped Si. There are 200-Å undoped $Si/Si_{0.8}Ge_{0.2}$ spacer layers graded to p^+-Si contact regions on either side of the active region. We have fabricated device mesas down to a lateral extent of 5 μm using conventional metallization and etching techniques.[15] When a bias V is applied between the contact regions at low temperatures T, current flows by hole tunneling from the valence band of the strained $Si_{0.8}Ge_{0.2}$ emitter region into the coupled subbands of the $Si_{0.8}Ge_{0.2}$ double-well structure.

Figure 1 shows a typical tunneling $I(V)$ characteristic for a triple-barrier RTS with $L=20$ Å, which exhibits well-resolved resonant peaks at $V=215$ and 500 mV. The higher-bias peak is considerably stronger, and all three RTS's we have measured have a similar strong high-bias resonance at $V\approx 500$ mV. The self-consistent potential profile[16] of the active region of the $L=20$-Å structure at $V=500$ mV, shown in the inset of Fig. 1, demonstrates that at such high values of applied bias the top of the collector barrier falls below the Fermi level in the emitter. Therefore, we attribute this resonance to tunneling from the emitter to the LH_0 subband in

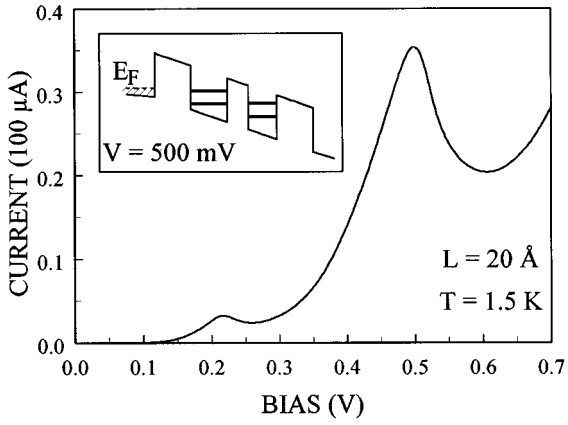

FIG. 1. Tunneling $I(V)$ characteristics at $T=1.5$ K of triple-barrier RTS's with a middle-barrier width $L=20$ Å. The inset gives the self-consistent potential distribution for $V=500$-mV applied bias, indicating HH_0 and LH_0 energy subbands in each well calculated in the absence of interwell coupling.

the first well, and then directly to the collector. Transport thus reduces to the extensively examined double-barrier case.[3–6] Since we are interested in coupled subband tunneling, we will restrict the rest of our analysis to the lower-bias range, $V \leqslant 400$ mV.

The lower-bias $I(V)$ characteristics of the three structures are presented in Fig. 2. The triple-barrier RTS with $L=10$ Å exhibits resonant peaks at $V=175$, 265, and 345 mV, whereas the devices with $L=20$ and 30 Å each have a single peak at $V=215$ and 190 mV, respectively. Hence the most significant change in the spectroscopy pattern is observed when the middle barrier width is changed from 10 to 20 Å.

We model the $I(V)$ characteristics by applying the sequential tunneling model,[9] where we treat the 2D double-

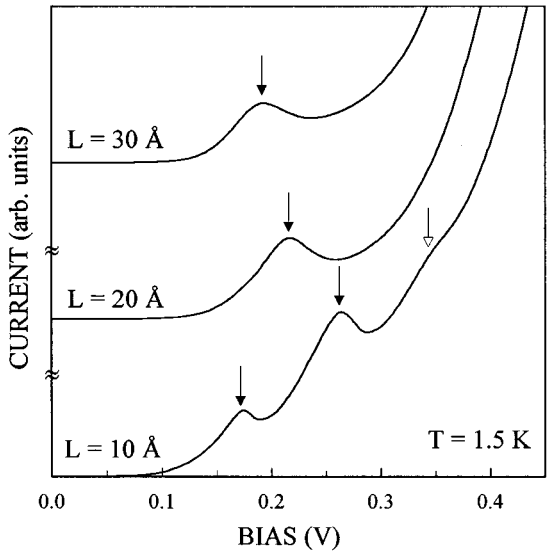

FIG. 2. Tunneling $I(V)$ characteristics at $T=1.5$ K of triple-barrier RTS's in the low-bias range for $L=10$, 20, and 30 Å. The $I(V)$ curves of the different structures have been rescaled and shifted for clarity. Solid arrows delineate the observed peak positions of the $HH_0^{(1)}$-$HH_0^{(2)}$ resonances, and the open arrow delineates the $HH_0^{(1)}$-$LH_0^{(2)}$ resonance.

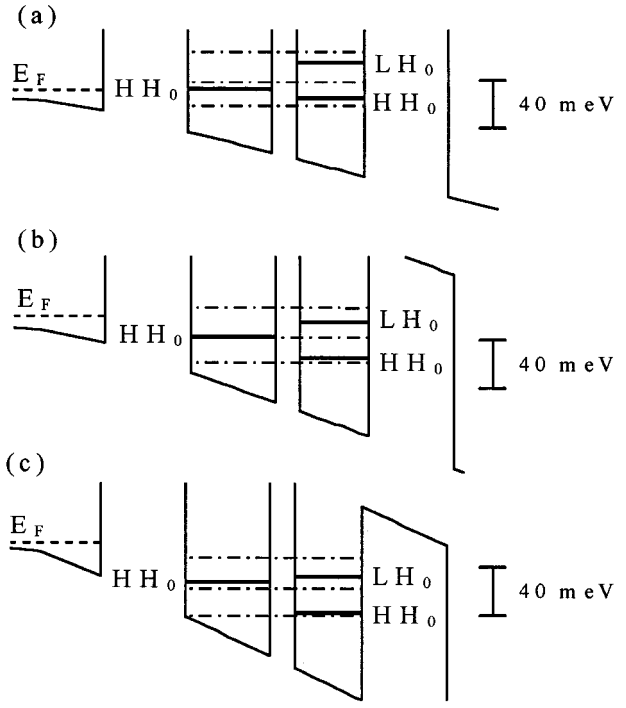

FIG. 3. Schematic valence-band diagrams of triple-barrier RTS's with a middle-barrier width $L=10$ Å at bias values corresponding to the experimentally measured resonances: (a) $V=175$ mV, (b) $V=265$ mV, and (c) $V=345$ mV. The dash-dotted line represents the double-well tunneling subbands. The LH_0 subband in the first well, which lies $\sim$35 meV above the HH_0 subband in the same well, has been omitted for clarity.

well subbands similarly to the ordinary quantized 2D subbands in double-barrier RTS's. At low T, only HH emitter states are occupied due to a strain-induced HH-LH splitting of about 40 meV in the emitter region.[17] Heavy holes tunnel from the emitter into a double-well subband, conserving energy E and transverse momentum $\mathbf{k}_\perp$,[9] and then into a suitable state in the collector region. The supply function $N(V)$ is defined as the number of holes satisfying the E and $\mathbf{k}_\perp$ tunneling selection rules, which depends on the alignment of the double-well subbands and the occupied emitter states. The tunneling current is then given by

$$I \propto N(V) T_e(V), \tag{1}$$

where $T_e(V)$ is the transmission coefficient through the first barrier. Because of charge accumulation near the emitter barrier of the RTS under bias (shown in Fig. 3), the peak current is expected to occur when the energy of the 2D subband falls somewhat below the bulk valence-band edge E_V in the emitter.[18]

The double-well wave functions can be expanded as linear combinations of the quantized eigenfunctions of two individual quantum wells and continuum states. In a first-order approximation, it is sufficient to include into this linear combination only a few single-well eigenfunctions whose energies are nearest to the energy of the double-well wave function of interest.[19] Figure 3 illustrates the band alignments for each of the three bias values at which resonance is observed in the $L=10$-Å RTS (see Fig. 2). In our calculation of the

double-well subbands, we have used HH and LH single-well subband energies calculated for $\mathbf{k}_\perp = \mathbf{0}$, incorporating strain effects and interpolated band-edge masses.[20] In the lower-bias range, $V \leqslant 400$ mV, the double-well wave functions $|\Psi_i\rangle$ relevant to hole tunneling can safely be approximated as a linear combination of the HH ground state of the first well, $|\mathrm{HH}_0^{(1)}\rangle$, and the HH and LH ground states in the second well, $|\mathrm{HH}_0^{(2)}\rangle$ and $|\mathrm{LH}_0^{(2)}\rangle$, respectively:

$$|\Psi_i\rangle = \alpha_i|\mathrm{HH}_0^{(1)}\rangle + \beta_i|\mathrm{HH}_0^{(2)}\rangle + \gamma_i|\mathrm{LH}_0^{(2)}\rangle, \qquad (2)$$

where α_i, β_i, and γ_i are functions of the applied bias V and the middle barrier width L. This is because the LH ground state of the first well, $|\mathrm{LH}_0^{(1)}\rangle$, lies $\sim$35 meV higher than the energy of the $|\mathrm{HH}_0^{(1)}\rangle$ state, and is not near enough in energy to have any significant interaction with the other subbands of the second well. Applying conventional techniques,[19] we calculate the double-well subband energies by evaluating the overlap integrals of the single-well wave functions of Eq. (2).

The prediction of positions of the resonant peaks in $I(V)$ data requires knowledge of the supply function $N(V)$, given by the area of a 2D surface in E-$\mathbf{k}_\perp$ space determined by the intersection of the occupied state distribution in the emitter and the available states in the double-well subbands given by $E_i(\mathbf{k}_\perp)$.[9] Generally, the functional form of $E_i(\mathbf{k}_\perp)$ requires numerical calculation, but we obtain approximate results by assuming simple parabolic dispersions. Our knowledge of the HH_0 subbands in SiGe quantum wells[13] is adequate to make reliable calculations of the $\mathrm{HH}_0^{(1)}$-$\mathrm{HH}_0^{(2)}$ coupling. On the other hand, the LH_0 subbands are much more complicated,[10,11] and we have chosen to treat the $\mathrm{HH}_0^{(1)}$-$\mathrm{LH}_0^{(2)}$ interaction strength, which depends strongly on the LH_0 effective mass away from $\mathbf{k}_\perp = \mathbf{0}$, as a fitting parameter.

Using the results shown in Fig. 3 for the $L = 10$-Å structure and analogous calculations for $L = 20$- and 30-Å RTS's, we can identify the resonant peaks in the $I(V)$ data of Fig. 2. We attribute the first two resonant peaks of the $L = 10$-Å RTS at $V = 175$ and 265 mV (marked with solid arrows in the lowest curve of Fig. 2) to tunneling into double-well subbands due primarily to $\mathrm{HH}_0^{(1)}$-$\mathrm{HH}_0^{(2)}$ coupling. The third peak of the same structure at $V = 345$ mV (marked with an open arrow in the lowest curve of Fig. 2) corresponds to a double-well subband created by $\mathrm{HH}_0^{(1)}$-$\mathrm{LH}_0^{(2)}$ coupling (see Fig. 3). The weakness of the $V = 345$-mV resonant peak indicates that the $\mathrm{HH}_0^{(1)}$-$\mathrm{LH}_0^{(2)}$ coupling is weak compared to the $\mathrm{HH}_0^{(1)}$-$\mathrm{HH}_0^{(2)}$ coupling. As the middle barrier width L increases, the $\mathrm{HH}_0^{(1)}$-$\mathrm{LH}_0^{(2)}$ interaction becomes even weaker, and an analogous peak becomes too weak to observe in the $L = 20$- and 30-Å RTS's. The energy of the double-well subband involved in the first resonant tunneling peak of the $L = 10$-Å RTS is closest to the $\mathrm{HH}_0^{(2)}$ energy level; hence the corresponding double-well wave function is concentrated in the second well adjacent to the collector barrier. As L increases, the concentration of this wave function in the first well becomes very small, and the transmission coefficient decreases sharply as the middle barrier width is increased from 10 to 20 Å. Therefore, the first resonant tunneling peak of the $L = 10$-Å RTS is also not observable in the $L = 20$- and 30-Å RTS. We conclude that the first peaks of the $L = 20$- and 30-Å RTS's at $V = 265$ and 190 mV, respectively (marked with solid arrows in the upper curves of Fig. 2), are due to tunneling into the higher-energy double-well subband created by $\mathrm{HH}_0^{(1)}$-$\mathrm{HH}_0^{(2)}$ coupling, and correspond to the second peak of the $L = 10$-Å RTS.

According to our model, the increase of the middle barrier width will affect the observed higher-energy $\mathrm{HH}_0^{(1)}$-$\mathrm{HH}_0^{(2)}$ resonant tunneling peak common to all three RTS's by means of the following two major contributions. First, as L increases from 10 to 20 Å, the $\mathrm{HH}_0^{(1)}$-$\mathrm{LH}_0^{(2)}$ interaction becomes very small, and further increasing L to 30 Å has a negligible effect on the spectroscopy pattern. Hence the energy of the upper $\mathrm{HH}_0^{(1)}$-$\mathrm{HH}_0^{(2)}$ subband should increase as L increases from 10 to 20 Å, and we expect the corresponding peak to shift to larger bias. Second, the considerably stronger $\mathrm{HH}_0^{(1)}$-$\mathrm{HH}_0^{(2)}$ coupling gradually decreases as L increases from 10 to 20 to 30 Å with the opposite effect of shifting the corresponding resonance peak toward lower-bias values. Our observations display a clear downward shift of the higher-energy $\mathrm{HH}_0^{(1)}$-$\mathrm{HH}_0^{(2)}$ resonant peak for increasing middle barrier width L, implying that the $\mathrm{HH}_0^{(1)}$-$\mathrm{HH}_0^{(2)}$ coupling contribution to triple-barrier resonant tunneling spectroscopy is much stronger than $\mathrm{HH}_0^{(1)}$-$\mathrm{LH}_0^{(2)}$ coupling.

Our calculations based on parabolic dispersion relations predict that the higher-energy $\mathrm{HH}_0^{(1)}$-$\mathrm{HH}_0^{(2)}$ resonant tunneling peak should shift to lower bias as the middle barrier width increases from 10 to 20 Å, and should be observed at approximately the same bias in $L = 20$- and 30-Å devices. However, our measurements, presented in Fig. 2, show that this peak shifts to lower bias linearly with increasing L, and the shift in the bias position from $L = 10$ to 20 Å is larger than our prediction. Looking at the bias positions and line shapes of the resonant peaks at $V \approx 500$ mV due to double-barrier resonant tunneling observed in all three RTS's, we conclude that this unexpectedly large shift of the higher-energy $\mathrm{HH}_0^{(1)}$-$\mathrm{HH}_0^{(2)}$ double-well subband to a lower bias with increasing middle barrier width is not due to experimental artifacts like series resistance or leakage current. We believe that in order to fully understand this phenomenon, we

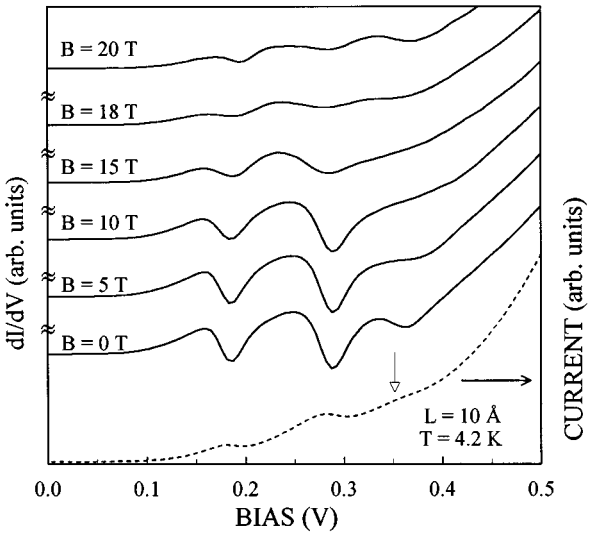

FIG. 4. Conductance dI/dV characteristics of the $L = 10$-Å triple-barrier RTS's at $B_\parallel = 0$, 5, 10, 15, 18, and 20 T. The dashed curve indicates $I(V, B_\parallel = 0)$ for comparison, with the open arrow indicating the $\mathrm{HH}_0^{(1)}$-$\mathrm{LH}_0^{(2)}$ resonance. The curves have been shifted for clarity.

need to incorporate nonparabolic in-plane dispersions into our model. Work on a more sophisticated model is currently in progress.

Another spectroscopic tool that has proven useful in the study of quantum-well subbands is the magnetic field. In double-barrier p-Si/$Si_{1-x}Ge_x$ RTS's, parallel field magnetotunneling $I(V,B_{\|})$ measurements have been used to study the intriguing Landau-level spectra.[6,21] In order to observe the Landau structure of coupled subbands, we have completed a set of preliminary $I(V,B_{\|})$ measurements on our triple-barrier RTS's. Figure 4 shows the conductance dI/dV characteristics of the $L=10$-Å structure for fields up to $B_{\|}=20$ T measured at 4.2 K. We observe a marked decrease in the relative intensity of the HH-LH resonance at $V=345$ mV (indicated by the open arrow in Fig. 4) as $B_{\|}$ increases, until resonance is no longer observed for $B_{\|}\geqslant 10$ T. As the magnetic field increases further, an additional peak emerges at a similar bias. It remains for further study, including $I(V,B_{\|})$ measurements at higher magnetic fields, to determine whether this peak is due to the reemergence of the HH-LH coupling, Landau index nonconserving tunneling,[21] or some other mechanism.

In conclusion, we have experimentally observed $I(V)$ peaks corresponding to tunneling through coupled 2D HH-HH and HH-LH subbands in strained p-Si/$Si_{1-x}Ge_x$ asymmetric triple-barrier RTS's with various middle barrier widths. By application of a simple wave-function formalism describing these double-well subbands, we are able to identify these peaks, including a peak due to tunneling through a subband arising from weak HH-LH interwell coupling. Further, we have presented intriguing preliminary magnetotunneling results demonstrating quenching of the HH-LH resonance peak and the possible emergence of satellite peaks for fields up to $B_{\|}=20$ T.

We are pleased to acknowledge the assistance of J. P. Cheng and the Francis Bitter National Magnet Lab staff. This material is based upon work partially supported by the National Science Foundation under the Materials Research Group (Grant No. DMR-9121747) and the ONR Young Investigator Program (Grant No. N00014-95-1-0729).

[1] R. People, IEEE J. Quantum Electron **QE-22**, 1696 (1986).
[2] J. C. Bean, Proc. IEEE **80**, 571 (1992).
[3] H. C. Liu, D. Landheer, M. Buchanan, and D. C. Houghton, Appl. Phys. Lett. **52**, 1809 (1988).
[4] U. Gennser, V. P. Kesan, S. S. Iyer, T. J. Bucelot, and E. S. Yang, J. Vac. Sci. Technol. B **9**, 2059 (1991).
[5] K. L. Wang, J. Park, S. S. Rhee, R. P. Karunasiri, and C. H. Chern, Superlatt. Microstruct. **5**, 201 (1989).
[6] G. Schuberth, G. Abstreiter, E. Gornik, F. Schäffler, and J. F. Luy, Phys. Rev. B **43**, 2280 (1991).
[7] L. L. Chang, L. Esaki, and R. Tsu, Appl. Phys. Lett. **24**, 593 (1974).
[8] E. E. Mendez, W. I. Wang, B. Ricco, and L. Esaki, Appl. Phys. Lett. **47**, 415 (1985).
[9] S. Luryi, Appl. Phys. Lett. **47**, 490 (1985).
[10] R. Wessel and M. Altarelli, Phys. Rev. B **40**, 12 457 (1989).
[11] U. Ekenberg and M. Altarelli, Phys. Rev. B **32**, 3712 (1985).
[12] U. Gennser, V. P. Kesan, D. A. Syphers, T. P. Smith III, S. S. Iyer, and E. S. Yang, Phys. Rev. Lett. **67**, 3828 (1991).
[13] A. Zaslavsky, T. P. Smith III, D. A. Grützmacher, S. Y. Lin, T. O. Sedgwick, and D. A. Syphers, Phys. Rev. B **48**, 15 112 (1993).
[14] T. Nakagawa, H. Imamoto, T. Kojima, and K. Ohta, Appl. Phys. Lett. **49**, 73 (1986); Y. Zohta, T. Nozu, and M. Obara, Phys. Rev. B **39**, 1375 (1989).
[15] A. Zaslavsky, D. A. Grützmacher, Y. H. Lee, W. Ziegler, and T. O. Sedgwick, Appl. Phys. Lett. **61**, 2872 (1992).
[16] Calculated using the HETMOD software package written by A. C. Warren of IBM Research.
[17] R. People, Phys. Rev. B **32**, 1405 (1985).
[18] V. J. Goldman, D. C. Tsui, and J. E. Cunningham, Phys. Rev. B **35**, 9387 (1987).
[19] G. Bastard, *Wave Mechanics Applied to Semiconductor Heterostructures* (Halsted, New York, 1988), Chap. 1.
[20] X. Xiao, C. W. Liu, J. C. Sturm, L. C. Lenchyshyn, and M. L. W. Thewalt, Appl. Phys. Lett. **60**, 2135 (1992).
[21] A. Zaslavsky, D. A. Grützmacher, S. Y. Lin, T. P. Smith III, R. A. Kiehl, and T. O. Sedgwick, Phys. Rev. B **47**, 16 036 (1993).